Connect with experts and peers through Special Interest Groups, a searchable member directory, and interactive events.

Stay informed with online access to *Prenatal Diagnosis* journal, *Global Updates* e-newsletter, and position statements.

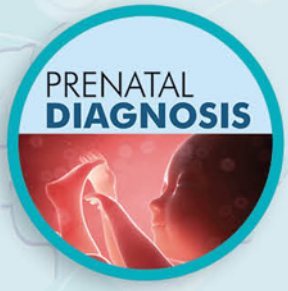

Learn through webinars, the International Conference on Prenatal Diagnosis and Therapy, interviews with experts, and recorded talks.

Professional membership is available for medical and allied health professionals.

Trainee membership is complimentary and includes access to Early Career Resources.

Visit **www.ispdhome.org** for details.

ispd International Society for Prenatal Diagnosis

Building Global Partnerships in Genetics and Fetal Care

ispd education

ISPD is a global society of professionals and trainees from disciplines such as prenatal and perinatal care, medical genetics, basic and translational science, genetic counseling, laboratory management, fetal therapy, ultrasonography, and ethics. Become a member today at **www.ispdhome.org/join**.

www.ispdhome.org info@ispdhome.org +1 434.979.4773

Check for updates

Received: 6 February 2018 | Revised: 7 May 2018 | Accepted: 28 May 2018

DOI: 10.1002/pd.5292

ORIGINAL ARTICLE

WILEY PRENATAL DIAGNOSIS

The third ventricle of the human fetal brain: Normative data and pathologic correlation. A 3D transvaginal neurosonography study

Roee Birnbaum[1] | Stefano Parodi[2] | Gloria Donarini[1] | Gabriella Meccariello[1] | Ezio Fulcheri[3] | Dario Paladini[1]

[1] Istituto G. Gaslini, Fetal Medicine and Surgery Unit, Genoa, Italy

[2] Istituto Giannina Gaslini, Unit of Epidemiology, Biostatistics and Committees, Genoa, Italy

[3] Istituto G. Gaslini, Pathology Unit, Genoa, Italy

Correspondence
Dario Paladini, Fetal Medicine and Surgery Unit, Istituto G. Gaslini, Genoa, Italy.
Email: dpaladini49@gmail.com

Abstract

Objective: The objective of the study are to describe (a) the technical aspects and (b) the anatomical boundaries of the fetal third ventricle (3V) on the midsagittal sonographic view and to assess (c) different biometric parameters in normal and abnormal fetuses and (d) and their reproducibility.

Methods: This study included 67 normal and 50 CNS anomalies fetuses which include (1) obstructive severe ventriculomegaly (SVM; atrial width ≥ 15 mm), (2) moderate ventriculomegaly (10-14.9 mm), and (3) corpus callosum agenesis (ACC). All underwent transvaginal 3D neurosonography of the midsagittal view of the 3V. The following parameters were measured: area, perimeter, craniocaudal and anteroposterior (AP) diameters, interthalamic adhesion diameter (ITAD), wedge angle, and the ratio between the last 2 variables (ITAD/WA). Repeatability was also assessed.

Results: The ITAD and the ITAD/WA are significantly different between normal fetuses and the SVM ($P \leq .001$). Interthalamic adhesion diameter of ≤7.1 mm is able to identify SVM with 98.6% accuracy (CI: 0.92-0.99). In ACC cases, the AP diameter is significantly shorter than both normal fetuses and ventriculomegaly. Intraobserver/interobserver reliability was good for most variables.

Conclusions: Transvaginal neurosonography enables visualization of the normal and abnormal fetal third ventricle. An ITAD <7.1 identifies aqueductal stenosis as the likely etiology of severe ventriculomegaly with an accuracy of 98.6%.

1 | INTRODUCTION

The third ventricle of the human brain provides luminal continuity between the 2 lateral ventricles and the cerebral aqueduct. It is a narrow vertical cleft, located in the midline, wedged in between the 2 thalami, and connected to the lateral ventricles by the Monro foramina. It has a roof, represented by the tela choroidea, located under the body of the fornix; a floor, made up by the hypothalamus and the subthalamus, in addition to the optic chiasm; an anterior wall, constituted by the lamina terminalis; and a posterior one, formed by the pineal stalk and the habenular commissures. The third ventricle has an irregularly trapezoidal shape and several recesses.[1] Of all the recesses, the preoptic recess, located in the sharp angle between the lower edge of the lamina terminalis and the back of the optic chiasm, is of note, because this area, together with the lamina terminalis, is involved in early changes in the case of obstructive hydrocephalus.[2,3]

In the neonate, the normal and abnormal aspects of the third ventricle have been mainly described on MR, and to a lesser extent on ultrasound (US).[4,5] In particular, neonatal nomograms of the third ventricular width, measured both in the coronal and axial planes by using transfontanelle ultrasound, have been published.[4,6,7] In the fetus, ultrasound studies of the third ventricle of the brain are scarce.

 © 2018 John Wiley & Sons, Ltd.

Hertzberg et al[8] and Sari et al[9] published 2 longitudinal studies of the normal width and configuration of the third ventricle. Both these studies focused on the area between the thalami on the axial plane view of the fetal head as displayed on transabdominal 2-dimensional (2D) US, and showed consistent results.

However, to the best of our knowledge, no attempt has been made so far to study the anatomy of the third ventricle on a midsagittal view of this structure obtained with high-resolution transvaginal 3D US. We think that, because of the unique shape and irregular borders of the third ventricle, only this approach is able to show its peculiar anatomic details in normal and abnormal conditions. It should also be considered that the anatomy of the third ventricle is distorted in a series of major central nervous system congenital and acquired conditions. Therefore, identification of its morphological changes is of key importance for a definite diagnosis of these anomalies.

The objectives of this study are (a) to assess and describe the technical aspects of the fetal third ventricle imaging on the midsagittal view; (b) to describe the anatomical boundaries of the third ventricle and its depiction using 3D US in normal fetuses in the second half of pregnancy; (c) to assess different biometric parameters in normal fetuses and compare these values to fetuses with ventriculomegaly, to verify their contribution for the differential diagnosis of ventriculomegaly (VM) cases; and (d) to assess the intraobserver and interobserver reliability of the newly proposed biometrical parameters.

What's already known about this topic?

- The third ventricle of the fetal brain is a complex-shaped lumen, connecting the lateral and fourth ventricles. Brain malformations may change its geometry in various aspects, but these aspects do not show up on the axial view. Normative data in the fetus are scarce and include only the axial plan view.

What does this study add?

- We describe the midsagittal view of the third ventricle and its normal anatomic surroundings, by high-resolution transvaginal neurosonography. We assess its biometry and aspect in normal fetuses and fetuses with ventriculomegaly from different etiologies.

2 | MATERIALS AND METHODS

Design and population

This is a mixed prospective and retrospective cross-sectional study conducted between May 2016 and April 2017, and approved by our Institutional Review Board. The normative study includes a group of 67 normal fetuses (controls) prospectively assessed in the study period. The pathology group includes a set of 50 fetuses with 1 of the 3 following conditions: (a) mild isolated VM (atrial width: 10.0-14.9 mm), (b) severe VM (atrial width: ≥15 mm), and (c) complete agenesis of the corpus callosum. Thirty of these 50 cases were managed at our unit during the study period and, hence, prospectively evaluated; the remaining 20 had been seen over the last 10 years, and assessed retrospectively. For the third group, only cases in which 3D volume datasets were available and acquired according to the specifications illustrated below were included. In the first group, all patients underwent routine obstetric scan, after which they were invited to participate in the study. After signing an informed consent, patients underwent transvaginal 3-dimensional neurosonography (3D-NSG). In the second group, ie, patients with CNS malformations, after a comprehensive evaluation of extra-CNS anatomy (including echocardiography) carried out with a transabdominal approach, 3D-NSG was performed for diagnostic purposes. Final diagnosis was available in all cases, by means of autopsy or postnatal magnetic resonance imaging (MRI). The 50 study group fetuses were allotted to 3 different categories according to the final diagnosis: (1) primary obstructive severe VM (atrial width > 15 mm) (12 cases), (2) mild isolated VM (atrial width 10-14.9 mm; 16 cases), and (3) complete agenesis of the corpus callosum (ACC: 22 cases). It should be underlined that cases were considered for the study and included in group 1 only if the cause of obstruction was aqueductal stenosis.

Gestational age was determined on the basis of the last menstrual period (LMP), confirmed by at least 1 previous sonographic examination performed during the first trimester. Redating was done according to current guidelines.[10] For the purpose of the study, weeks + days were considered in the statistical analysis. Furthermore, a fetus was considered as "normal" if growth was consistent with dating at the time of scanning (no IUGR) and early neonatal assessment was unremarkable.

Ultrasound methodology and measurements

In all cases, 3D-NSG was performed with volumetric transducers, using a 6 to 12 MHz array until 24 gestational weeks (GW) and a 5 to 9 MHz one from 25 GW onwards, to warrant more penetration (Voluson 730 Expert, E6, E8, E10, GE Healthcare, Milwaukee, IL). Each fetus was included only once in the study. After diagnostic assessment of brain anatomy, 3D volumetric datasets were obtained according to the methodology described below. Two authors (either DP or RB) acquired the volumes.

As far as the used methodology, which is described below, there are 2 issues which need be clarified. First of all, we attempted visualization of the third ventricle in several ways, on 3D-NSG, from the posterior fontanelle to the anterior one with various insonation angles; the only approach which is effective in displaying the third ventricle is with the tip of the transducer pointing directly toward this structure, through the anterior fontanelle. In all other cases, the reflection and deflection of ultrasound waves hampers its visualization. At this regard, we assessed also the success/failure rate in obtaining the above-described plane in the prospectively evaluated group of normal fetuses. The second methodological issue regards the use of 3-dimensional ultrasound and VCI. We tried to visualize the third ventricle on the native A window image without adding the VCI, which

corresponds to the 2-dimensional approach, and failed repeatedly to display this anatomical structure. Despite its slit-like appearance, the use of VCI with 1-mm thickness enhances conspicuously the edge recognition, leading to adequate identification of the third ventricle shape and anatomical boundaries (Figures 1–3).

As for the sonographic methodology in details, its first step consists in positioning the transvaginal transducer in such a way to indent the anterior fontanelle, to warrant a transfontanellar approach[11] in all cases; this was obtained by manipulating the fetal head from the abdomen. Once the midsagittal view was obtained, a 3D volume

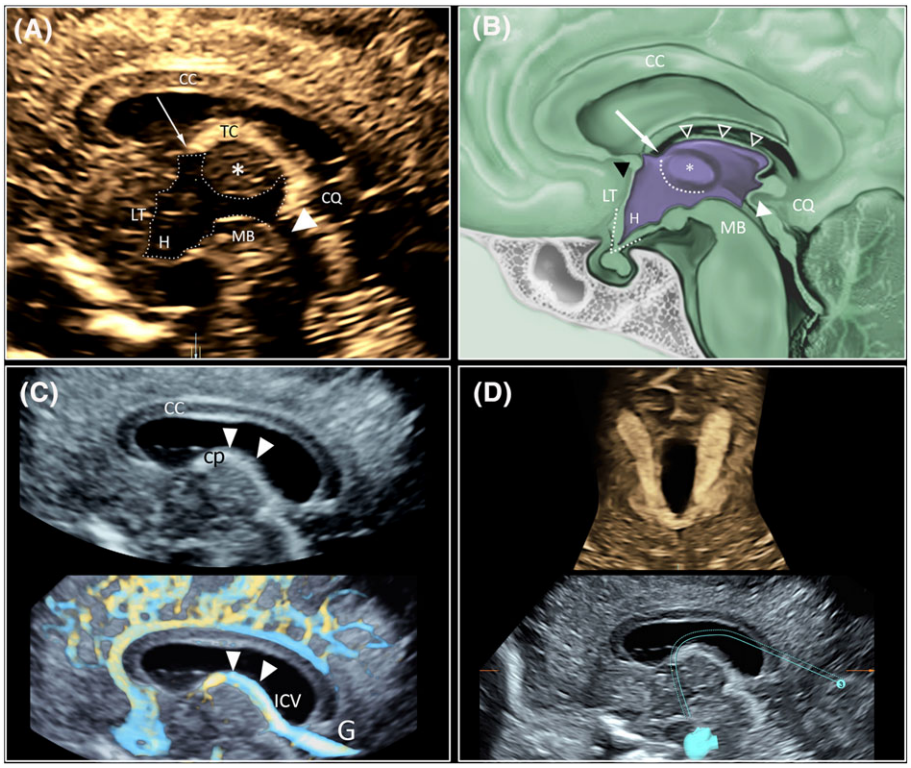

FIGURE 1 Three-dimensional transvaginal ultrasound of fetal brain at 28 gestational weeks. A, On multiplanar imaging + volume contrast imaging (see text for technical details), the anatomical landmarks of the third ventricle are shown (dashed white line: perimeter of the third ventricle; arrow: foramen of Monro; white arrowhead: Sylvian aqueduct; LT, lamina terminalis; H, hypothalamus; TC, tela choroidea; MB, mid-brain; CQ, cisterna quadrigemina; *interthalamic adhesion). B, An illustration showing major anatomic landmarks of the third ventricle and surroundings (arrow: foramen of Monro; black arrowhead: anterior commissure; blank arrowheads: roof with body of fornices and tela choroidea; white arrowhead: Sylvian aqueduct; *interthalamic adhesion; wedged dashed line: the area where infundibular and supraoptic recess converge with the anterior wall and floor; curved dashed line: ventral border of the interthalalmic adhesion; CC, corpus callosum; CQ, cisterna quadrigemina; MB, mid-brain; LT, lamina terminalis; H, hypothalamus). C, On 3-dimensional HD flow (lower panel) and volume contrast imaging (upper panel), the components of the roof of the third ventricle are shown (arrowheads: tela choroidea and choroid plexus (cp); G, vein of Galen; ICV, internal cerebral vein). D, On Omniview, tracing a curved line joining the choroid plexuses of the lateral ventricles to the third ventricle on the midline (lower panel) and the continuity between the lateral and third ventricular choroid plexuses are demonstrated (upper panel)

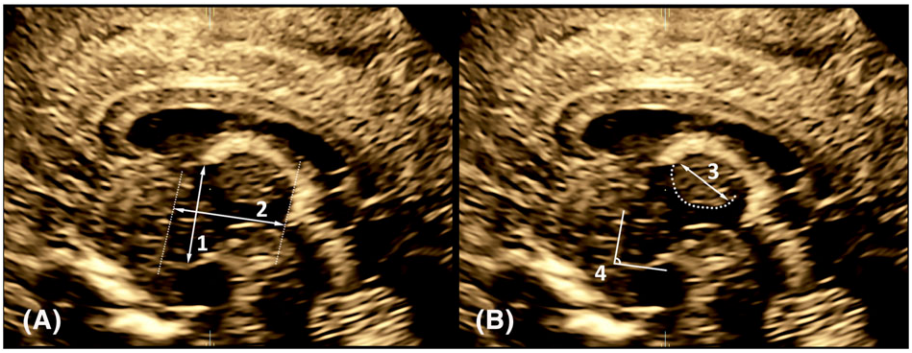

FIGURE 2 Third ventricle sonographic measurements (for definitions see text). A, Craniocaudal diameter (1) and anteroposterior diameter (2). B, Maximum diameter of the interthalamic adhesion (ITAD) (3) and wedge angle (4)

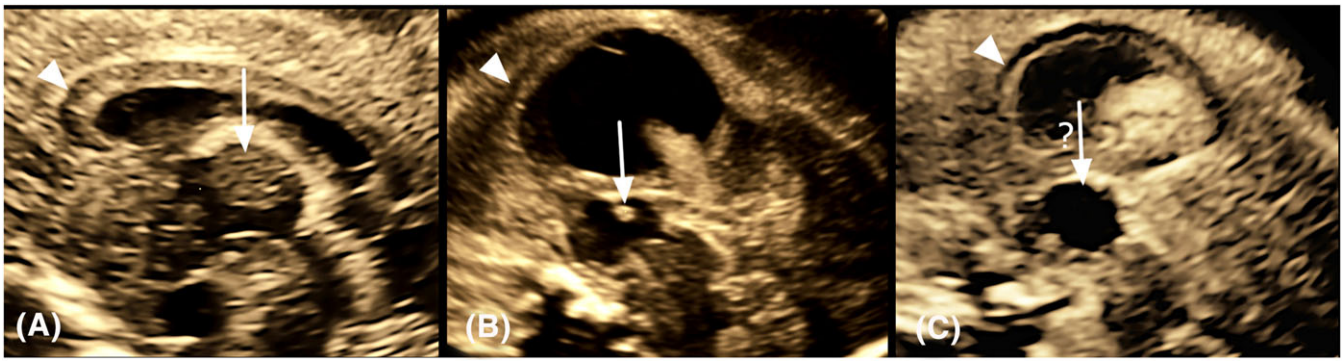

FIGURE 3 Midsagittal view of the third ventricle on 3-dimensional multiplanar imaging + volume contrast imaging (1 mm). The interthalamic adhesion (ITA, arrow) is normal size in a (normal fetus, 32 gestational weeks), reduced in B (primary severe ventriculomegaly, 28 gestational weeks), absent (?) in C (primary severe ventriculomegaly, 24 gestional weeks). Arrowhead: corpus callosum

dataset (quality: maximum; angle: 40°-50°) was acquired and stored. If any fetal movement was detected during or after the acquisition, the dataset was discarded. All 3D volume datasets were then processed offline according to the following protocol. A dedicated software was used (4D view, version 14, General Electrics, Milwaukee, IL). Each volume was uploaded, and multiplanar image correlation was used together with volume contrast imaging (slice thickness of 1 mm). After aligning the 3 orthogonal planes, the sagittal view of the third ventricle was displayed on the A window. The following anatomic landmarks, bordering the third ventricle, were identified prior to measurements (Figure 1A, B): (a) *anterior wall*: it is represented by the *lamina terminalis* (Figure 1A), extending from the wedge-shaped area of the infundibular and supraoptic recess ventrally, to the area where the anterior commissure, foramen of Monro with the choroid plexus, and the lower border of septum pellucidum converge, dorsally; (b) *roof*—formed by the hyperechoic complex of the body of the fornix and the *tela choroidea* with its choroid plexus and vessels (Figure 1A-D); (c) *interthalamic adhesion* (ITA, Figure 1A, B)—the curved ventral border of the oval ITA extends from the roof to the caudal section of the posterior wall. The latter is marked by the echogenic line separating the third ventricle from the *cisterna quadrigemina*. It should be noted that, although anatomically the lumen of the third ventricle potentially encircle the ITA both ventrally and dorsally, the dorsal lumen is visible only in some pathologic cases where the lumen is enlarged. Hence, for methodological purposes, we used the readily visible curved ventral border of the ITA for all normative measurements: (d) *floor* (Figure 1A, B): the ventral border of the third ventricle evolves posteriorly from the upper margin of the *mesencephalon* (ie, upper midbrain) where the third ventricle funnels into the cerebral aqueduct, and extend anteriorly through the *diencephalon* in a wedge configuration formed by the hypothalamus (including *mammillary* area posteriorly and *tuber cinereum* and *infundibular* area anteriorly). Rostrally, the floor converge with the anterior wall.

All images were processed and measurements taken by a first operator (RB). To assess the reproducibility, 20 cases were randomly selected and measurements taken by a second operator (DP) and a second time by the first operator, both blinded to the results of the other evaluations. The following measurements were taken: (1) area and perimeter of the third ventricle: this measurement was performed by tracing a continuous line along the anatomical borders described earlier and measuring the enclosed area and trace line length (Figure 1A); (2) craniocaudal diameter (CCD) of the third ventricle, defined as the distance between the lower edge of the choroid plexus on the roof of the third ventricle and the lowermost portion of the floor (Figure 2A); (3) anteroposterior diameter (APD) of the third ventricle, defined as the distance between a line placed along the anterior wall, and a corresponding parallel one crossing through the posterior margin of the third ventricular lumen (Figure 2A); (4) ITA diameter, defined as the maximum diameter of the ITA (ITAD) (Figure 2B); and (5) the wedge angle (WA), defined as the angle between a line drawn along the anterior wall landmarks and a second line drawn along the floor of third ventricle to its lowermost point, close to the anterior wall (Figure 2B). In addition, the ratio between the ITAD and the WA was calculated (ITAD/WA).

Statistics

Comparison of frequency data was performed by the mean of the chi-square test or the Fisher exact test when appropriate. The Mann-Whitney *U* test was used to compare median values. The diagnostic accuracy of the considered measures was estimated by the method of the ROC curves adjusted for the effect of gestational age and the presence of repeated measures on the same individual.[12] The relation between each measure and gestational age was also evaluated in the control group by polynomial regression analysis including linear, quadratic, and cubic terms for the independent variable. Each model was fitted restricting the analyses to the control group, and the estimated coefficients were applied to the whole study population to obtain marker values standardized by gestational age.[13]

Repeatability was assessed by calculating the intraclass correlation coefficient (ICC) for intraobserver and interobserver reliability.[14] The latter was estimated comparing measures from the first operator to the average of the 2 series of available measures from the second one. The Bland and Altman method and the Pitman's test were applied to evaluate the corresponding agreement between measures both between and within operator.[15,16]

All the analyses were carried out with the Stata for Windows statistical package (release 13.1, Stata Corporation, College Station, TX).

TABLE 1 Low-degree polynomial regression models analyzing the association between each considered measure and gestational age in the control group

Parameter	Coeff.	t	P	F	R^2
Area				51.03	0.634
Gestational age—linear term	0.023	3.29	.002		
Gestational age—quadratic term	−0.00005	−2.55	.013		
Perimeter				93.34	0.760
Gestational age—linear term	0.074	3.46	.001		
Gestational age—quadratic term	−0.00013	−2.44	.018		
Wedge				103.44	0.618
Gestational age—linear term	0.004	10.17	<.001		
CC diameter				78.57	0.711
Gestational age—linear term	0.031	4.69	<.001		
Gestational age—quadratic term	−0.00007	−3.82	<.001		
AP diameter				138.26	0.680
Gestational age—linear term	0.0049	11.76	<.001		
ITAD				164.66	0.717
Gestational age—linear term	0.005	12.83	<.001		
Wedge angle				11.43	0.322
Gestational age—linear term	25.3	2.42	.019		
Gestational age—quadratic term	−0.1322	−2.43	.018		
Gestational age—cubic term	0.00022	2.39	.020		
ITAD/WA				108.17	0.628
Gestational age—linear term	0.0002	10.40	<.001		

Only statistically significant terms are retained in the final model.

Coeff., regression coefficient; t, ratio between the regression coefficient and the corresponding standard error; AP diameter, anteroposterior diameter; CC diameter, craniocaudal diameter; ITAD, interthalamic adhesion diameter; ITAD/WA, interthalamic adhesion diameter/wedge angle ratio.

3 | RESULTS

Mean maternal age at ultrasound was 32.3 (SD 5.1 years, range: 21-40). Mean gestational age at ultrasound was 27 weeks + 2 days (SD 4 weeks + 6 days, range: 19-39 weeks) for the study and 28 weeks + 0 days (SD 3 weeks + 5 days, range: 20-35 weeks) for the control group (P = .288).

Considering the feasibility of the proposed approach, we assessed the success/failure rate in the prospectively assessed group of normal fetuses. We were able to obtain the ideal approach in 67/74 (90.5%) pregnancies in which it was attempted. In the 7 remaining cases, the approach failed because of failed version in breech fetuses (4 cases), unfavorable nonmodifiable position of the fetal head during examination (2 cases), and maternal low compliance to TV scanning (1 case).

Table 1 summarizes the best equation to represent the relationships between the analyzed variables and gestational age. The scatterplots showing the relationships between each considered variable and gestational age for the control group and the 3 abnormal categories are shown in Figures S1 to S7 in the supporting information. In brief, all variables show a positive linear correlation with advancing

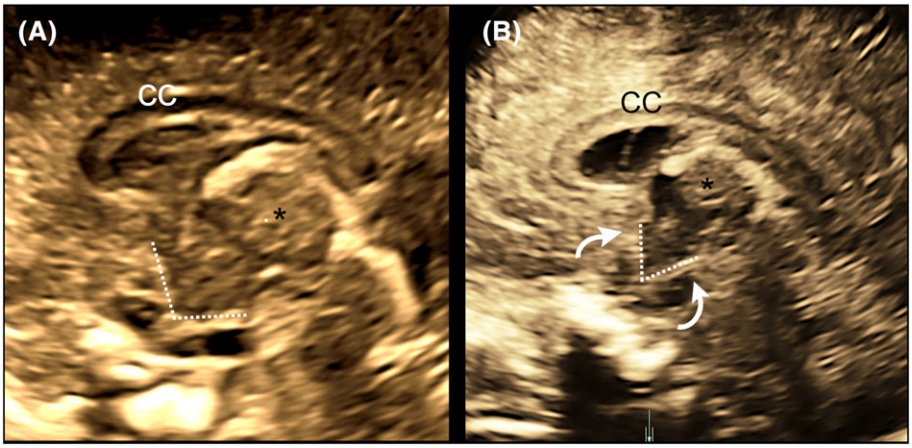

FIGURE 4 Gestation-related changes in the aspect of the third ventricle. Midsagittal view of the third ventricle. A, A wide wedge angle between the floor and anterior wall is present at 22 gestational weeks (dashed lines). B, At 32 weeks, the same angle is significantly reduced, because of coming together of the floor and anterior wall (dashed lines)

gestational age but the wedge angle, for which there is a negative correlation; in fact, it decreases with advancing gestational age. This was also the major developmental change with advancing gestational age (Figure 4), which is seen only on the midsagittal view, whereas the axial one remains virtually unchanged, considering that the change involves the anterior and basal aspects of the third ventricle. As for the measurements, it was not possible to measure all parameters in all cases, as evident from Table 2, which shows comparison of the 3 categories of the study group with the control one. In particular, the AP diameter of the third ventricle is shorter in cases of ACC and severe isolated VM. The ITAD is also significantly smaller in all pathologic cases. However, the ITAD—as well as the ITAD/WA median—values are exceedingly smaller in the case of primary severe obstructive VM than in any other category ($P < .001$; Table 2; Figures S6A and S7A; Figure 3). At this regard, it should be added that the ITAD could not be measured in 3 of the 15 cases of primary severe obstructive VM (≥15 mm) because the ITA was absent, because of disconnection (Figure 3C).

TABLE 2 Median and interquartile ranges (IQR) for all variables, adjusted for gestational age (see text for details)

	N	Median	IQR	*P*
Area (cm^2)				
Controls	62	0.82	0.76-0.89	Ref.
Atrium ≥15 mm	11	0.91	0.78-1.0	.143
Atrium <15 mm	16	0.85	0.75-0.95	.287
Agenesis of corpus callosum	19	0.77	0.70-0.88	.181
Perimeter (cm)				
Controls	62	4.9	4.7-5.1	Ref.
Atrium ≥15 mm	11	5.0	3.9-5.4	.890
Atrium <15 mm	16	4.7	4.4-5.0	.128
Agenesis of corpus callosum	19	4.9	4.1-5.2	.490
CC diameter (cm)				
Controls	67	1.1	1.0-1.2	Ref.
Atrium ≥15 mm	12	1.1	0.98-1.3	.869
Atrium <15 mm	16	1.1	1.0-1.2	.926
Agenesis of corpus callosum	21	1.1	1.0-1.3	.856
AP diameter (cm)				
Controls	67	1.52	1.46-1.57	Ref.
Atrium ≥15 mm	11	1.39	1.17-1.47	.004
Atrium <15 mm	16	1.45	1.38-1.55	.060
Agenesis of corpus callosum	20	1.39	1.37-1.44	<.001
Wedge angle (°)				
Controls	67	69.8	64.1-77.9	Ref.
Atrium ≥15 mm	10	79.1	63.0-93.5	.243
Atrium <15 mm	16	74.4	65.6-85.1	.288
Agenesis of corpus callosum	19	71.6	57.8-84.9	.735
ITAD (cm)				
Controls	67	0.89	0.84-0.93	Ref.
Atrium ≥15 mm	7	0.54	0.32-0.62	<.001
Atrium <15 mm	16	0.80	0.74-0.91	.011
Agenesis of corpus callosum	20	0.80	0.72-0.85	<.001
ITAD/WA[a]				
Controls	66	1.3	1.1-1.4	Ref.
Atrium ≥15 mm	6	0.43	0.26-1.1	.001
Atrium <15 mm	16	1.0	0.91-1.3	.003
Agenesis of corpus callosum	13	1.3	1.1-1.4	.570

AP diameter, anteroposterior diameter; CC diameter, craniocaudal diameter; ITAD, interthalamic adhesion diameter; ITAD/WA, interthalamic adhesion diameter/wedge angle ratio.

[a]×100.

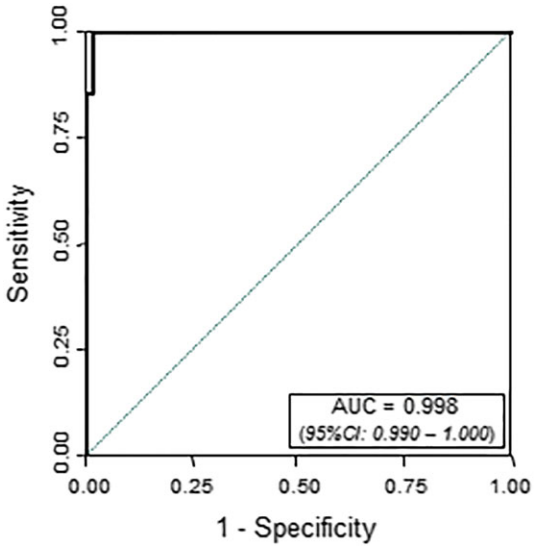

FIGURE 5 Receiver operator curves (ROC) for the interthalamic adhesion diameter (ITAD) adjusted for gestational age (see text for methodology). The area under the curve (AUC) is 0.998 [Colour figure can be viewed at wileyonlinelibrary.com]

The distribution of the ITAD on the ROC curves adjusted for gestational age is shown in Figure 5. A cutoff value of 7.1 mm or lower (Figure 6) is able to identify primary obstructive severe VM from normals and all other causes of VM with 98.6% accuracy (CI: 0.92-0.99).

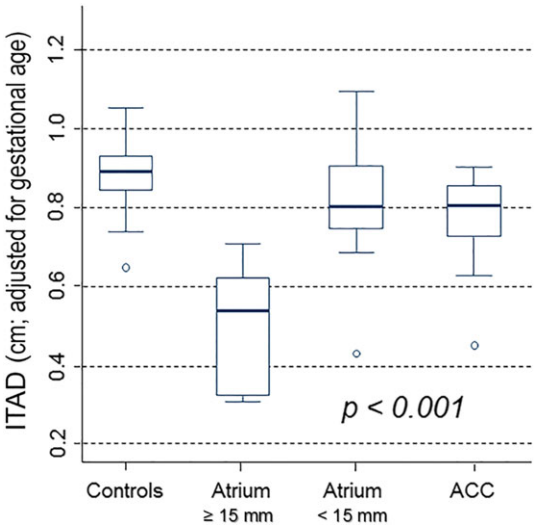

FIGURE 6 Box plot showing interthalamic adhesion diameter (ITAD) value in normal fetuses (controls) and fetuses with central nervous system (CNS) malformations by CNS category. (ACC, agenesis of corpus callosum). Circles represent outliers. As evident, ITAD is much smaller in fetuses with primary severe obstructive ventriculomegaly (atrium ≥15 mm), than in controls and all other categories [Colour figure can be viewed at wileyonlinelibrary.com]

TABLE 3 Intraobserver and interobserver reliability evaluated by the intraclass correlation coefficient (ICC)

	Intraobserver reliability		Interobserver reliability	
Parameter	ICC	95% CI	ICC	95% CI
Area	0.85	0.67-0.94	0.84	0.65-0.93
Perimeter	0.92	0.81-0.97	0.90	0.76-0.96
CC diameter	0.86	0.69-0.94	0.79	0.55-0.91
AP diameter	0.79	0.55-0.91	0.79	0.55-0.91
Wedge angle	0.92	0.82-0.97	0.91	0.79-0.96
ITAD	0.74	0.47-0.89	0.85	0.66-0.94

AP diameter, anteroposterior diameter; CC diameter, craniocaudal diameter; ITAD, interthalamic adhesion diameter; ITAD/WA, interthalamic adhesion diameter/wedge angle ratio.

ROC analysis results for all remaining variables are summarized in Table S1.

Results of the reliability analysis are shown in Table 3; Bland and Altman plots are reported in Figures S8 and S9 that also show the corresponding *P* values for the Pitman's test; the mean and 95% confidence intervals of agreement for Bland and Altman plots are shown in Table S2. No statistically significant value was found either for the intraoperator or interoperator agreement.

4 | DISCUSSION

In the existing literature, normative data on the sonographic aspect of the normal third ventricle of the brain in the human fetus are rather limited and regard only its axial aspect, as seen on transabdominal ultrasound.[8,9] To the best of our knowledge, an assessment of the anatomic landmarks of the third ventricle visible on its sagittal view has not been reported. In the present study, we describe the normal sonographic appearance of the boundaries of the third ventricle, as visible on the midsagittal view of the fetal head. In particular, most of the anatomic landmarks identified on MR in postnatal life are evident also on high-resolution 3D-NSG, as shown in this study (Figures 1–3). In addition, we report on its biometry, which shows a significant relationship with advancing gestational age (Table 1). At this regard, it should be noted that all parameters grow linearly with advancing gestation, with the exception of the WA, which significantly decreases (Figures 4 and S5). This dramatic change is visible only on the midsagittal view, because it involves mainly the anterior wall and the floor of the ventricle; the axial slit-like appearance remains unchanged. The subjective impression is that both the anterior wall and the floor of the third ventricle move one toward the other, determining a reduction of the angle.

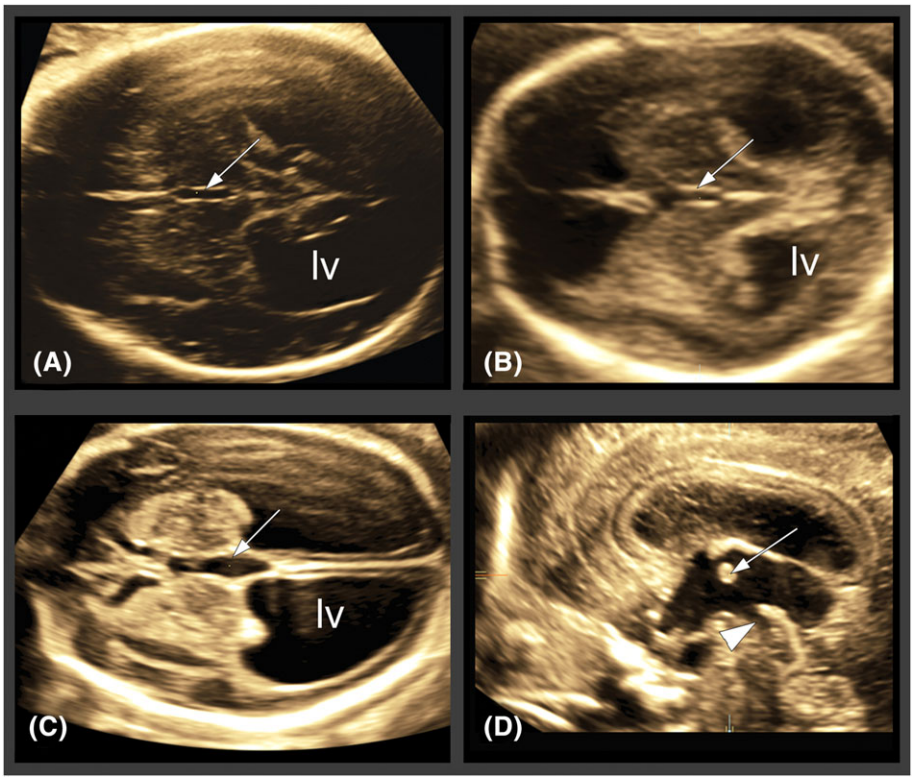

FIGURE 7 Axial aspect of the third ventricle in obstructive vs nonobstructive ventriculomegaly. A, Isolated nonobstructive ventriculomegaly (postnatal confirmation) at 30 gestational weeks. On the axial transventricular view, mild dilatation of the third ventricle and moderate ventriculomegaly (lv) are visible. B, Primary obstructive ventriculomegaly from aqueductal stenosis (postnatal confirmation) at 22 gestational weeks. On the transventricular view, the findings are rather similar to case A: moderate dilatation of the third ventricle and mild ventriculomegaly. C-D, Primary obstructive ventriculomegaly from aqueductal severe stenosis (postnatal confirmation) at 34 gestational weeks. On the transventricular view (C), dilatation of the third ventricle and severe ventriculomegaly are visible; on the midsagittal, transvaginal view of the fetal brain (D), the third ventricle is visible in detail, showing widening of the inferior portion, evagination of the posterior wall into the cisterna quadrigemina, thinning of the interthalamic adhesion (arrow) and slight dilatation of the aqueductal inlet (arrowhead), followed by obstruction

Another objective of the study was to analyze whether and how any of the assess biometric parameters contribute to the differential diagnosis of VM. The reason why our primary objective was obstructive VM is because of a couple of reasons. First of all, it remains challenging to make a prospective diagnosis of "primary obstructive ventriculomegaly (hydrocephalus)" in the fetus; despite some recent evidence,[17,18] this diagnosis represents still, in most cases, an "exclusion diagnosis": when no other cerebral anomalies possibly responsible for VM are found on 3D-NSG, this represents the more likely diagnosis. In fact, other than a rather unspecific dilatation of the third ventricle, the axial view cannot provide significant insight into the etiology of VM, considering also that the aqueduct is barely visible and, hence, evaluable, on the axial view (Figure 7). In the third trimester, prenatal brain MRI may support this diagnosis by showing nonvisualization or obstruction of the Sylvian aqueduct, even though a recent article has demonstrated how the aqueduct can indeed be studied on transvaginal ultrasound as well.[18] In this study, Vinals et al visualized and measured the Sylvian aqueduct in a series of 206 normal cases, and failed to see it in a set of 7 cases with a postnatal diagnosis of aqueductal stenosis. This study is interesting, and represents an alternative approach to ours, which focuses on the third ventricle rather than the aqueduct. There is also another study addressing the shape of the third ventricle in obstructive VM, underlining how in these cases a dilatation of the suprapineal recess might represent a sensitive sign[19]; however, Azzi et al[19] did not perform a comprehensive study on the third ventricle as we do in the present investigation. The reason why we focused on this anatomic structure is because a recent series of neuroendoscopy reports describe how the third ventricle anatomy is distorted in obstructive hydrocephalus.[2,3] Also, in postnatal life, MRI shows that in aqueductal stenosis, the ITA is smaller, probably because of both compression from the relatively high pressure of the cerebrospinal fluid in the third ventricle and to stretching from an increased coronal tension[3]; in some cases of severe obstructive hydrocephalus, the ITA can even disappear, probably because of disjunction of the adhesion.[20] In the present study, we demonstrate that also in the fetus with severe obstructive VM, the ITA is smaller and, in a few cases, absent (Figure 3C).

In ACC, the main feature is a different shape of the third ventricle (reduced AP diameter; Table 3 and Figure S4) with the ITAD and the WA less affected, as shown by the unchanged ITAD/WA ratio (Figure S7). It is possible to speculate that, in normal cases, it is the extent of crossing callosal fibers that elongate the third ventricle anteroposteriorly, on the sagittal plane; when these are absent, as in ACC, the hollow third ventricle is somewhat less mandated to grow anteroposteriorly, leading to a reduction of the AP diameter.

A final comment regards the reliability analysis, which showed fair intraobserver and interobserver reliability for all measurements.

This study has significant limitations. First of all, the gestational age range is limited. This is because of both technical problems with visualization of the third ventricle before and after the analyzed gestational age span and to the fact that most abnormal cases were managed in the same range of weeks, so that it made sense to limit the study to the same gestational period. Secondly, the number of normal cases examined (67) is not large enough to warrant production of normative biometric charts. The fact that the present study required a significant extension of the scanning time because of the need for vaginal scanning was trivial neither for the examiner nor for the patient. Finally, the number of cases in the 3 categories of the study group is, again, rather limited.

In conclusion, we have demonstrated that the anatomic landmarks of the cerebral third ventricle can be visualized also in the fetus, on the midsagittal view of the fetal brain on 3D-NSG. We have also shown that the ITAD and, to a lesser extent, the ITAD/WA ratio are selectively smaller in primary severe obstructive VM. In particular, an ITAD <7.1 identifies obstruction (aqueductal stenosis) as the likely etiology of severe VM with an accuracy of 98.6%. This parameter may contribute to the prospective diagnosis of aqueductal stenosis in fetuses referred for 3D-NSG because of severe VM.

ORCID

Roee Birnbaum http://orcid.org/0000-0003-1073-6348

REFERENCES

1. O'Rahilly R, Muller F. *The embryonic human brain*: An atlas of developmental stages. Third ed. John Wiley & Sons, INC. publications; 2005.
2. Foroughi M, Wong A, Steinbok P, Singhal A, Sargent MA, Cochrane DD. Third ventricular shape: A predictor of endoscopic third ventriculostomy success in pediatric patients. *J Neurosurg Pediatrics*. 2011;7(4):389-396.
3. Dlouhy BJ, Capuano AW, Madhavan K, Torner JC, Greenlee JDW. Preoperative third ventricular bowing as a predictor of endoscopic third ventriculostomy success. *J Neurosurg Pediatrics*. 2012;9(2):182-190.
4. Sondhi V, Gupta G, Gupta PK, Patnaik SK, Tshering K. Establishment of nomograms and reference ranges for intra-cranial ventricular dimensions and ventriculo-hemispheric ratio in newborns by ultrasonography. *Acta Paediatr*. 2008 Jun;97(6):738-744.
5. Sarı E, Sarı S, Akgün V, et al. Measures of ventricles and evans' index: From neonate to adolescent. *Pediatr Neurosurg*. 2015;50(1):12-17.
6. Davies MW, Swaminathan M, Chuang SL, Betheras FR. Reference ranges for the linear dimensions of the intracranial ventricles in preterm neonates. *Arch Dis Child Fetal Neonatal Ed*. 2000 May;82(3):F218-F223.
7. Hartenstein S, Bamberg C, Proquitté H, Metze B, Bührer C, Schmitz T. Birth weight-related percentiles of brain ventricular system as a tool for assessment of posthemorrhagic hydrocephalus and ventricular enlargement. *J Perinat Med*. 2016 Mar;44(2):179-185.
8. Hertzberg BS, Kliewer MA, Freed KS, et al. Third ventricle: Size and appearance in normal fetuses through gestation. *Radiology*. 1997 Jun;203(3):641-644.
9. Sari A, Ahmetoglu A, Dinc H, et al. Fetal biometry: Size and configuration of the third ventricle. *Acta Radiol*. 2005 Oct;46(6):631-635.
10. Salomon LJ, Alfirevic Z, Bilardo CM, et al. ISUOG practice guidelines: Performance of first-trimester fetal ultrasound scan. *Ultrasound Obstet Gynecol*. 2013 Jan;41(1):102-113.
11. International Society of Ultrasound in Obstetrics & Gynecology Education Committee. Sonographic examination of the fetal central nervous system: Guidelines for performing the 'basic examination' and the 'fetal neurosonogram. *Ultrasound Obstet Gynecol*. 2007 Jan;29(1):109-116.
12. Janes H, Longton GM, Pepe MS. Accommodating covariates in receiver operating characteristic analysis. *Stata Journal*. 2009;9(1):17-39.
13. Kleinbaum DG, Kupper LL, Muller KE, Nizam A. *Applied regression analysis and other multivariable methods*. 3rd ed. Pacific Grove (CA): Duxbury Press; 1998:281-316.

14. Shrout PE, Fleiss JL. Intraclass correlations: Uses in assessing rater reliability. *Psychol Bull*. 1979;86(2):420-428.
15. Bland JM, Altman DG. Statistical methods for assessing agreement between two methods of clinical measurement. *Lancet*. 1986; 327(8476):307-310.
16. Bartlett JW, Frost C. Reliability, repeatability and reproducibility: Analysis of measurement errors in continuous variables. *Ultrasound Obstet Gynecol*. 2008;31(4):466-475.
17. Emery SP, Hogge WA, Hill LM. Accuracy of prenatal diagnosis of isolated aqueductal stenosis. *Prenat Diagn*. 2015;35(4):319-324.
18. Viñals F, Ruiz P, Quiroz G, et al. Two-dimensional ultrasound evaluation of the fetal cerebral aqueduct: Improving the antenatal diagnosis and counseling of Aqueductal stenosis. *Fetal Diagn Ther*. 2017; 42(4):278-284.
19. Azzi C, Giaconia MB, Lacalm A, Massoud M, Gaucherand P, Guibaud L. Dilatation of the supra-pineal recess on prenatal imaging: Early clue for obstructive ventriculomegaly downstream of the third ventricle. *Prenat Diagn*. 2014 Apr;34(4):394-401.
20. El Damaty A, Langner S, Schroeder HW. Ruptured Massa intermedia secondary to hydrocephalus. *World Neurosurg* 2017; 97:749.e7–749.e749.e10.

SUPPORTING INFORMATION

Additional supporting information may be found online in the Supporting Information section at the end of the article.

How to cite this article: Birnbaum R, Parodi S, Donarini G, Meccariello G, Fulcheri E, Paladini D. The third ventricle of the human fetal brain: Normative data and pathologic correlation. A 3D transvaginal neurosonography study. *Prenatal Diagnosis*. 2018;38:664–672. https://doi.org/10.1002/pd.5292